

Dynamics of ultracold molecules in confined geometry and electric field

Goulven Quéméner and John L. Bohn

JILA, University of Colorado, Boulder, CO 80309-0440, USA

(Dated: May 29, 2018)

We present a time-independent quantum formalism to describe the dynamics of molecules with permanent electric dipole moments in a two-dimensional confined geometry such as a one-dimensional optical lattice, in the presence of an electric field. Bose/Fermi statistics and selection rules play a crucial role in the dynamics. As examples, we compare the dynamics of confined fermionic and bosonic polar KRb molecules under different confinements and electric fields. We show how chemical reactions can be suppressed, either by a “statistical suppression” which applies for fermions at small electric fields and confinements, or by a “potential energy suppression”, which applies for both fermions and bosons at high electric fields and confinements. We also explore collisions that transfer molecules from one state of the confining potential to another. Although these collisions can be significant, we show that they do not play a role in the loss of the total number of molecules in the gas.

I. INTRODUCTION

Experimental evidence for ultracold chemistry of quantum-state controlled molecules [1] and dipolar collisions in the quantum regime [2] has been obtained recently for fermionic KRb molecules in the lowest electronic, vibrational, rotational quantum state [3] and well-defined hyperfine states [4]. Bosonic species of KRb have also been formed recently [5] as well as other alkali polar molecules such as RbCs [6] and LiCs [7]. The exoergic reaction $\text{KRb} + \text{KRb} \rightarrow \text{K}_2 + \text{Rb}_2$ [8–10] prevents long trap lifetimes of these molecules, especially in electric fields, where the chemical reactivity increases as the sixth power of the dipole moment induced by the electric field [2, 11]. Lifetimes are then typically of the order of 10 ms for experimental electric fields. However, polar molecules offer long range and anisotropic dipolar interactions in electric fields. If the molecules are confined in optical lattices, they can be stabilize against collisions and chemical reactions [12–17], if the dipoles are polarized in the direction of a tight confinement. If these molecules are confined into the ground state of a realistic one dimensional optical lattice, electric field suppression of chemical reactions is expected to occur, yielding lifetimes of KRb molecules of $\simeq 1$ s and elastic scattering rates 100 times more efficient than chemical reaction rates [15, 16]. Both of these are needed to achieve molecular evaporative cooling and to reach the quantum regime where the phase-space density is high. For fermionic molecules, creation of degenerate Fermi gases of dipoles will likely be possible. In case of bosonic molecules, Bose–Einstein condensates can instead be formed. This will reveal exciting physics with ultracold controlled molecules in the quantum regime [18–21].

We address in this paper two important points regarding collisions in a lattice. First, suppression of confined chemical reactions in electric fields can be obtained by using the centrifugal repulsion of fermionic molecules in the same internal state (electronic, vibrational, rotational and spin) and in the same confining state of the one dimensional optical lattice. The centrifugal re-

pulsion comes from the statistics of identical fermions in indistinguishable states. This requires only comparatively small dipoles and weak confinements. Suppression that relies directly on the confining potential and the repulsion due to electric dipoles can also be obtained, but requires larger dipoles and stronger confinements. It does, however, suppress both bosons and fermions, in indistinguishable states or not, or even for different polar molecules.

Secondly, realistic experimental dynamics of polar molecules in confined geometry is more complicated than the ideal case used in the recent theoretical works [15, 16], where only molecules in the ground state of the lattice were considered. Realistically, molecules can also be formed in excited states of the optical lattice, depending for example on the temperature, the strength of the confinement, and the way the optical lattice is turned on [22]. It is therefore important to know how rapidly collisions can populate higher confining states, which could after all, contribute to re-thermalization; and how do the molecules in these excited states affect the loss rate of the total molecules. These questions are important for ongoing experiments of KRb molecules in an optical lattice [22].

In this article, we extend the formalism developed in our former work [15]. We describe in section II the dynamics of molecules in an arbitrary initial confining state of the lattice, and consider the possibility for the molecules to leave such a state for another after a collision. In section III, we show how chemical reaction can be suppressed for fermionic and bosonic KRb molecules under different confinements and electric fields. In section IV, we discuss the importance of inelastic collisions of molecules in different confining states. Finally, we conclude in section V.

In the following, quantities are expressed in S.I. units, unless explicitly stated otherwise. Atomic units (a.u.) are obtained by setting $\hbar = 4\pi\epsilon_0 = 1$.

II. THEORETICAL FORMALISM

In this section, we explain the theoretical formalism we use. Former studies have dealt with collisions in two dimensions [14–17, 23, 24] but were restricted to small confinements or assumed no transitions between confining states. In the present formalism, we have no such restrictions. Our method is based on a frame transformation between spherical to cylindrical coordinates, similar to that employed in Ref. [25, 26] for example. The frame transformation has the advantage of treating in full detail the microscopic physics of the molecule-molecule interaction, while projecting onto appropriate two dimensional scattering states. We consider two ultracold polar molecules of masses m_1, m_2 and positions \vec{r}_1, \vec{r}_2 from a fixed arbitrary origin O (see Fig. 1-a). The molecules are confined in a harmonic oscillator trap $V_{\text{ho}}^\tau = m_\tau \omega^2 z_\tau^2/2$ for molecule $\tau = 1, 2$, of angular frequency $\omega = 2\pi\nu$. An electric field applied along the confinement direction \hat{z} polarizes the molecules, giving them dipole moments $\vec{d}_\tau = d_\tau \hat{z}$. We use cartesian coordinates (x_τ, y_τ, z_τ) to describe the vector \vec{r}_τ . We also use the center-of-mass (CM) coordinate $\vec{R} = (m_1\vec{r}_1 + m_2\vec{r}_2)/(m_1 + m_2)$ and the relative coordinate $\vec{r} = \vec{r}_2 - \vec{r}_1$ (see Fig. 1-a). We use the cartesian coordinate (X, Y, Z) to describe the vector \vec{R} , and either cylindrical coordinates (ρ, z, φ) or spherical coordinates (r, θ, φ) to describe the vector \vec{r} (see Fig. 1-b), with $\rho = r \sin \theta$ and $z = r \cos \theta$. Both the electric field and the harmonic oscillator potential are applied along the z axis, which we take as the quantization axis.

A. Hamiltonian

The total Hamiltonian of the system is

$$H_{\text{tot}} = T_1 + T_2 + V \quad (1)$$

with $T_\tau = -\hbar^2 \nabla_{\vec{r}_\tau}^2 / (2m_\tau)$ representing the kinetic energy operator of the molecule τ . V , the potential energy, is given by

$$\begin{aligned} V &= V_{\text{abs}} + V_{\text{vdW}} + V_{\text{dd}} + V_{\text{ho}}^{\tau=1} + V_{\text{ho}}^{\tau=2} \\ &= iAe^{-(r-r_{\text{min}})/r_c} - \frac{C_6}{r^6} + \frac{d_1 d_2 (1 - 3 \cos^2 \theta)}{4\pi\epsilon_0 r^3} \\ &+ \frac{1}{2} \left(m_1 \omega^2 z_1^2 + m_2 \omega^2 z_2^2 \right). \end{aligned} \quad (2)$$

The first term on the right hand side represents an appropriate imaginary potential capturing the overall chemical couplings at short-range. It replaces ab initio calculations of the electronic structure of trimer and tetramer alkali complexes, which remain incomplete for KRb [8–10, 27]. For the time being, an absorbing potential has shown very good agreement with experimental results [1, 2, 31, 32] for KRb molecules. We use the same absorbing potential here. The second term represents an isotropic van der Waals interaction ; the third term

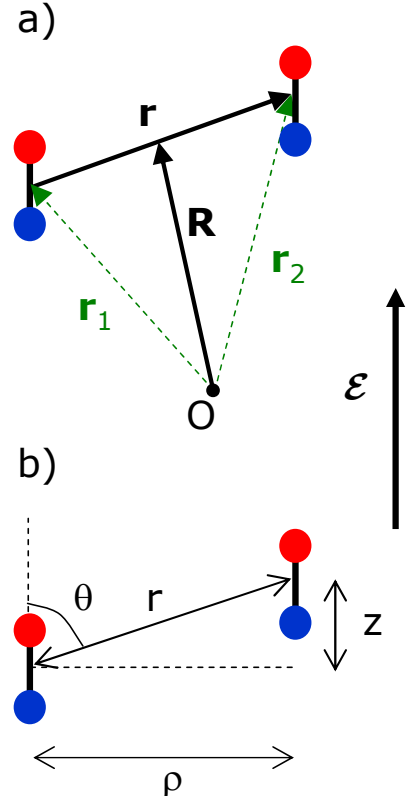


FIG. 1: (Color online) a) Position vectors of the molecules. The electric field is along the z direction. b) Spherical coordinates (r, θ) and cylindrical coordinates (ρ, z) of the relative coordinate. We suppose $\varphi = 0$ in the picture.

represents the dipole-dipole interaction where d_τ represents the expectation value in the z direction of the dipole moment induced by the electric field ; and the last two terms represent the one dimensional harmonic oscillator trap that confines the molecules in a plane perpendicular to the z direction. The initial energy of the molecule τ in the trap is given by $\epsilon_{n_\tau} = \hbar\omega(n_\tau + 1/2)$, where n_τ represents the associated quantum number of the harmonic oscillator state they are loaded into. The associated function is the usual normalized eigenfunction of the harmonic oscillator $g_{n_\tau}(z_\tau)$.

B. Symmetrized internal and external states

We consider here identical molecules with same masses ($m_1 = m_2$) and same dipoles ($d_1 = d_2 = d$). As the molecules are identical, we have to construct an overall wavefunction Ψ of the system for which the molecular

permutation operator P gives

$$P \Psi = \epsilon_P \Psi \quad (3)$$

with $\epsilon_P = +1$ for bosonic molecules and $\epsilon_P = -1$ for fermionic molecules. This overall wavefunction Ψ is constructed from an internal wavefunction $|\alpha_1 \alpha_2\rangle$ representing the electronic, vibrational, rotational and spin degrees of freedom of molecule 1 and 2 respectively; from an external wavefunction $|n_1 n_2\rangle$ representing the one dimensional individual confining wavefunction $g_{n_1}(z_1) g_{n_2}(z_2)$; and finally from a two dimensional collision wavefunction in the plane perpendicular to the confinement.

We first build symmetrized states of the internal wavefunction

$$|\alpha_1 \alpha_2, \eta\rangle = \frac{1}{\sqrt{2(1 + \delta_{\alpha_1, \alpha_2})}} \left[|\alpha_1 \alpha_2\rangle + \eta |\alpha_2 \alpha_1\rangle \right] \quad (4)$$

for which $P |\alpha_1 \alpha_2, \eta\rangle = \eta |\alpha_1 \alpha_2, \eta\rangle$. η is a good quantum number and is conserved during the collision. If the molecules are in the same molecular internal state, only the symmetry $\eta = +1$ has to be considered. If they are in different internal state, both symmetries $\eta = \pm 1$ have to be considered. We omit explicit reference to the internal wavefunctions $|\alpha_1 \alpha_2, \eta\rangle$ in the following, but the quantum number η still plays a role in the selection rules, as discussed in Appendix C.

We next build symmetrized states of the external confining wavefunction

$$|n_1 n_2, \gamma\rangle = \frac{1}{\sqrt{2(1 + \delta_{n_1, n_2})}} \left[|n_1 n_2\rangle + \gamma |n_2 n_1\rangle \right] \quad (5)$$

with $P |n_1 n_2, \gamma\rangle = \gamma |n_1 n_2, \gamma\rangle$. γ is a good quantum number and is conserved during the collision. If the molecules are in the same external confining state, only the symmetry $\gamma = +1$ has to be considered. If they are in different external state, both symmetries $\gamma = \pm 1$ have to be considered. It is useful at this point to turn into a relative/CM representation of the confining states. It is easy to show that the Hamiltonian (1) can also be written in the relative/CM representation as

$$H_{\text{tot}} = T_{\text{rel}} + T_{\text{CM}} + V_{\text{abs}} + V_{\text{vdW}} + V_{\text{dd}} + V_{\text{ho}}^{\text{rel}} + V_{\text{ho}}^{\text{CM}} \quad (6)$$

with $T_{\text{rel}} = -\hbar^2 \nabla_{\vec{r}}^2 / (2\mu)$ and $T_{\text{CM}} = -\hbar^2 \nabla_{\vec{R}}^2 / (2m_{\text{tot}})$, $\mu = m_1 m_2 / (m_1 + m_2)$ and $m_{\text{tot}} = m_1 + m_2$, $V_{\text{ho}}^{\text{rel}} = \mu \omega^2 z^2 / 2$ and $V_{\text{ho}}^{\text{CM}} = m_{\text{tot}} \omega^2 Z^2 / 2$. The associated energies and functions will be denoted ϵ_n, ϵ_N and $g_n(z), g_N(Z)$. These harmonic oscillator states in the relative and CM coordinates are related to those in independent particle coordinates $g_{n_1}(z_1), g_{n_2}(z_2)$ by (see

Appendix A)

$$g_{n_1}(z_1) g_{n_2}(z_2) = \frac{1}{\sqrt{2^{2(n_1+n_2)} n_1! n_2!}} \frac{\sum_{k=0}^{n_1} \sum_{k'=0}^{n_2} \sum_{q=0}^{\min(k, k')} \sum_{q'=0}^{\min(n_1-k, n_2-k')} \frac{n_1! n_2!}{(k-q)! (k'-q)! q! (n_1-k-q)! q'! (n_2-k'-q)!} \times (-1)^{n_1-k} 2^q 2^{q'} \sqrt{2^n n!} \sqrt{2^N N!} g_n(z) g_N(Z) \quad (7)$$

with

$$\begin{aligned} n &= -2q' + n_1 + n_2 - k - k' \\ N &= -2q + k + k'. \end{aligned} \quad (8)$$

We give in Appendix A explicit relations between $|n_1 n_2\rangle$ and $|n, N\rangle$ states for low values of quantum numbers, $0 \leq n_1, n_2 \leq 2$, and in Appendix B the relations between the symmetrized individual representation $|n_1 n_2, \gamma\rangle$ and the relative/CM representation $|n, N\rangle$ states, using Eq. (7) and Eq. (5).

C. Diabatic-by-sector method

To solve the Schrödinger equation for Ψ , we work in the relative/CM representation $|n, N\rangle$ since we know how to come back to the physical $|n_1 n_2, \gamma\rangle$ representation. In the relative/CM representation, the collisional problem depends only on the coordinate Z and the relative vector \vec{r} , and not on the coordinates X and Y . In the following, we explicitly remove these two coordinates from the problem. If we use the coordinate Z and spherical coordinates to represent \vec{r} , the Hamiltonian is given by

$$H = -\frac{\hbar^2}{2\mu} \frac{1}{r^2} \frac{\partial}{\partial r} \left(r^2 \frac{\partial}{\partial r} \right) + \frac{\hat{L}^2}{2\mu r^2} + V_{\text{abs}} + V_{\text{vdW}} + V_{\text{dd}} + V_{\text{ho}}^{\text{rel}} - \frac{\hbar^2}{2m_{\text{tot}}} \frac{\partial^2}{\partial Z^2} + V_{\text{ho}}^{\text{CM}}. \quad (9)$$

If we use the coordinate Z and cylindrical coordinates to represent \vec{r} , the Hamiltonian is given by

$$H = -\frac{\hbar^2}{2\mu} \left\{ \frac{\partial^2}{\partial \rho^2} + \frac{1}{\rho} \frac{\partial}{\partial \rho} + \frac{1}{\rho^2} \frac{\partial^2}{\partial \varphi^2} \right\} + V_{\text{abs}} + V_{\text{vdW}} + V_{\text{dd}} - \frac{\hbar^2}{2\mu} \frac{\partial^2}{\partial z^2} + V_{\text{ho}}^{\text{rel}} - \frac{\hbar^2}{2m_{\text{tot}}} \frac{\partial^2}{\partial Z^2} + V_{\text{ho}}^{\text{CM}}. \quad (10)$$

In a diabatic-by-sector method [28–30], using a spherical coordinate representation of the wavefunction, the range over the Schrödinger equation to be solved, $r_{\text{min}} \leq r \leq r_{\text{max}}$, is divided into N_s sectors of width $\Delta r = (r_{\text{max}} - r_{\text{min}}) / N_s$. The middle of each sector corresponds to a grid point r_p , with $p = 1, \dots, N_s$. At each grid

point $r = r_p$, we use N_l normalized Legendre polynomials $P_L^{M_L}(\cos\theta)$ for a given value of M_L , the quantum number associated with the azimuthal projection of the orbital angular momentum \hat{L} on the z direction, to diagonalize the angular Hamiltonian $\mathcal{H}^{M_L,\eta}(r,\theta) = \hat{L}^2/(2\mu r^2) + V_{\text{abs}} + V_{\text{vdW}} + V_{\text{dd}} + V_{\text{ho}}^{\text{rel}}$ of the Hamiltonian in Eq. (9). The resulting eigenfunctions are the adiabatic functions $\chi_j^{M_L,\eta}(r_p;\theta)$ with $j = 1, \dots, N_l$. They are used as a basis set for the representation of the total wavefunction

$$\Psi_j^{M_L,\eta,N}(r,\theta,\varphi,Z) = \frac{1}{r} \sum_{j''=1}^{N_{\text{adiab}}} \chi_{j''}^{M_L,\eta}(r_p;\theta) g_N(Z) F_{j''j}^{M_L,\eta,N}(r_p;r) \frac{e^{iM_L\varphi}}{\sqrt{2\pi}} \quad (11)$$

for a given adiabatic state j . The associated eigenenergies of the angular hamiltonian are the adiabatic energies $\varepsilon_j(r_p)$. They converge to the relative harmonic oscillator energies ε_n with $n = 0, \dots, N_l - 1$ at large r_p , so that a one-to-one correspondence can be identified between the adiabatic quantum states $j = 1, \dots, N_l$ and the relative harmonic oscillator quantum states $n = 0, \dots, N_l - 1$. In practice, we use a truncated number of adiabatic functions $N_{\text{adiab}} \ll N_l$. If we restrict the independent oscillator quantum numbers $0 \leq n_1, n_2 < n_{\text{osc}}^{\text{max}}$, then the maximum value that the relative quantum number n can take is $2n_{\text{osc}}^{\text{max}}$ and we choose $N_{\text{adiab}} = 2n_{\text{osc}}^{\text{max}}$. In Eq. (11), we use the fact that there are no terms in (9) that create mixings between different values of N . Moreover, the potential V does not depend on the azimuthal angle φ . As a consequence, the quantum numbers N and M_L are conserved during the collision.

The total energy E is equal to $\varepsilon_{n_1} + \varepsilon_{n_2} + E_c$, where $\varepsilon_{n_1}, \varepsilon_{n_2}$ are the energies of the molecules 1, 2 in the confining potential, when they start initially in n_1, n_2 , and E_c is the initial collision energy between the two molecules in the two dimensional plane. E is conserved during the collision. Solving the time-independent Schrödinger equation $H\Psi = E\Psi$ provides the following set of close-coupling differential equations in spherical coordinates for each values of M_L, η and N , from a state j to a state j'

$$\left\{ -\frac{\hbar^2}{2\mu} \frac{d^2}{dr^2} + \varepsilon_N - E \right\} F_{j'j}^{M_L,\eta,N}(r_p;r) + \sum_{j''=1}^{N_{\text{adiab}}} \mathcal{U}_{j'j''}^{M_L,\eta}(r_p;r) F_{j''j}^{M_L,\eta,N}(r_p;r) = 0 \quad (12)$$

where

$$\mathcal{U}_{j'j''}^{M_L,\eta}(r_p;r) = \int_0^\pi \chi_{j'}^{M_L,\eta}(r_p;\theta) \mathcal{H}^{M_L,\eta}(r,\theta) \chi_{j''}^{M_L,\eta}(r_p;\theta) \sin\theta d\theta. \quad (13)$$

The goal is to find all the elements $F_{j'j}^{M_L,\eta,N}$. We employ the standard method of the propagation of the log-

derivative matrix [33]

$$Z^{M_L,\eta,N}(r_p;r) = \left\{ (\partial/\partial r) F^{M_L,\eta,N}(r_p;r) \right\} \left\{ F^{M_L,\eta,N}(r_p;r) \right\}^{-1} \quad (14)$$

with matrix elements $Z_{j'j}^{M_L,\eta,N}(r_p;r)$, and obtain these elements for all possible states j to all possible states j' . In the diabatic-by-sector method, one has to perform a transformation operation from sectors to sectors, since the adiabatic functions $\chi^{M_L,\eta}(r_p;\theta)$ change from r_p to r_{p+1} . Then the log-derivative expressed in the basis of the sector $p+1$ at the distance $r = r_p + \Delta r/2$ separating the sector p and $p+1$ is given by

$$Z^{M_L,\eta,N}(r_{p+1};r = r_p + \Delta r/2) = P Z^{M_L,\eta,N}(r_p;r = r_p + \Delta r/2) P^{-1} \quad (15)$$

with the passage matrix

$$P_{j'j} = \int_0^\pi \chi_{j'}^{M_L,\eta}(r_{p+1};\theta) \chi_j^{M_L,\eta}(r_p;\theta) \sin\theta d\theta. \quad (16)$$

D. Asymptotic matching

Compared to free molecules in 3D, the external confinement $V_{\text{ho}}^{\text{rel}}$ in Eq. (9) persists at large intermolecular separation r , and the spherical representation of \vec{r} is not appropriate anymore. Instead, we use in the asymptotic region cylindrical coordinates appropriate to the potential $V_{\text{ho}}^{\text{rel}}$. For a given state of relative quantum number n , we now expand the total wavefunction as follows

$$\Psi_n^{M_L,\eta,\gamma,N}(\rho,z,\varphi,Z) = \frac{1}{\rho^{1/2}} \sum_{n''} g_{n''}(z) g_N(Z) G_{n''n}^{M_L,\eta,\gamma,N}(\rho) \frac{e^{iM_L\varphi}}{\sqrt{2\pi}}. \quad (17)$$

In the following, we will use the short-hand notation $\xi \equiv M_L, \eta, \gamma, N$. Note that because we use the coordinate Z and the wavefunction $g_N(Z)$ in both spherical and cylindrical representation, the external confinement $V_{\text{ho}}^{\text{CM}}$ is always well described. When $\rho \rightarrow \infty$, $V_{\text{abs}} + V_{\text{vdW}} + V_{\text{dd}} \rightarrow 0$, and the close-coupling asymptotic Schrödinger equations become

$$\left\{ -\frac{\hbar^2}{2\mu} \frac{d^2}{d\rho^2} + \frac{\hbar^2(M_L^2 - 1/4)}{2\mu\rho^2} + \varepsilon_n + \varepsilon_N - E \right\} G_{n'n}^\xi(\rho) = 0. \quad (18)$$

At large ρ , the radial function $G_{n'n}^\xi(\rho)$ in Eq. (17) is a linear combination of two possible solutions $G_{n'}^{\xi(1,2)}(\rho)$ of Eq. (18), and takes the form

$$G_{n'n}^\xi(\rho) \xrightarrow{\rho \rightarrow \infty} G_{n'}^{\xi(1)}(\rho) \delta_{n,n'} + G_{n'}^{\xi(2)}(\rho) K_{n'n}^\xi. \quad (19)$$

$K_{n'n}^\xi$ represents an element of the reactance matrix. The functions $G_{n'}^{\xi,(1,2)}$ represent the regular and irregular asymptotic solutions of the radial Schrödinger equation Eq. (18)

$$\begin{aligned} G_{n'}^{\xi,(1)}(\rho) &= \rho^{1/2} J_{M_L}(k_{n',N}\rho) \\ G_{n'}^{\xi,(2)}(\rho) &= \rho^{1/2} N_{M_L}(k_{n',N}\rho) \end{aligned} \quad (20)$$

where J_{M_L}, N_{M_L} are Bessel functions [38] and $k_{n',N} = \sqrt{2\mu(E - \varepsilon_{n'} - \varepsilon_N)}/\hbar$ is the wave number in the channel n' of the relative harmonic oscillator. If $E - \varepsilon_{n'} - \varepsilon_N < 0$, the modified Bessel functions have to be used instead.

To determine K , we must transform between the spherical wavefunction that captures the short-range physics and the cylindrical wavefunction that captures the asymptotic boundary conditions. The regular and irregular spherical radial functions $F_{j'}^{\xi,(1,2)}(r_p; r)$ and their derivatives can be connected to their cylindrical asymptotic counterpart $G_n^{\xi,(1,2)}(\rho)$ by equating the wavefunctions Eq. (11) and Eq. (17) and their derivatives at a constant sphere of radius $r = r_{\max}$

$$\begin{aligned} F_{j'j}^{\xi,(1,2)}(r_{p=N_s}; r) \Big|_{r=r_{\max}} &= \int_0^\pi \chi_{j'}^{M_L, \eta}(r_{p=N_s}; \theta) \\ &\frac{r}{\rho^{1/2}} g_n(z) G_n^{\xi,(1,2)}(\rho) \sin \theta d\theta \Big|_{r=r_{\max}} \end{aligned} \quad (21)$$

$$\begin{aligned} \frac{\partial}{\partial r} \left(F_{j'j}^{\xi,(1,2)}(r_{p=N_s}; r) \right) \Big|_{r=r_{\max}} &= \int_0^\pi \chi_{j'}^{M_L, \eta}(r_{p=N_s}; \theta) \\ &\frac{\partial}{\partial r} \left\{ \frac{r}{\rho^{1/2}} g_n(z) G_n^{\xi,(1,2)}(\rho) \right\} \sin \theta d\theta \Big|_{r=r_{\max}} \end{aligned} \quad (22)$$

with the one-to-one correspondence $\{n = 0, \dots, N_{\text{adiab}} - 1\} \equiv \{j = 1, \dots, N_{\text{adiab}}\}$ between the quantum numbers n and j . $r_{p=N_s}$ is the middle of the last sector N_s . This is a similar matching procedure that connects short-range democratic hyperspherical coordinates to asymptotic Jacobi coordinates employed in atom-molecule chemical reactive scattering studies [28–30]. Convergence with respect to N_{adiab} and r_{\max} is found when the Wronskian matrix

$$F^{\xi,(1)} \frac{\partial}{\partial r} \left(F^{\xi,(2)} \right) - \frac{\partial}{\partial r} \left(F^{\xi,(1)} \right) F^{\xi,(2)} \quad (23)$$

converges to the unit matrix.

The K matrix is determined by the matrix operation

$$K^\xi = -\frac{Z^\xi F^{\xi,(1)} - (\partial/\partial r)(F^{\xi,(1)})}{Z^\xi F^{\xi,(2)} - (\partial/\partial r)(F^{\xi,(2)})}. \quad (24)$$

The scattering matrix \mathcal{S} in the relative/CM representation is determined by

$$\mathcal{S}^\xi = \frac{I - iK^\xi}{I + iK^\xi} \quad (25)$$

where in this equation, I represents the unit matrix. The scattering matrix in the symmetrized individual representation $|n_1 n_2, \gamma\rangle$ is found by gathering all individual scattering matrices \mathcal{S} corresponding to different values of N and by applying a transformation from the relative/CM representation to the symmetrized individual representation

$$S^{M_L, \eta, \gamma} = U \left\{ \sum_N^\oplus \mathcal{S}^{M_L, \eta, \gamma, N} \right\} U^T. \quad (26)$$

The transformation matrix U , with elements $U_{n_1 n_2, \gamma; n, N} = \langle n_1 n_2, \gamma | n, N \rangle$, can be found using the relations in Appendix B. We use the transpose U^T of the matrix U instead of its inverse because U is not generally a square matrix.

E. Observables

After a collision, the quantum probability from an initial state $n_1 n_2$ to a final state $n'_1 n'_2$ for defined numbers M_L, η, γ is given by $P_{n'_1 n'_2, n_1 n_2}^{M_L, \eta, \gamma} = |S_{n'_1 n'_2, n_1 n_2}^{M_L, \eta, \gamma}|^2$. The elastic, inelastic (confining state changing) and reactive probabilities are given by

$$\begin{aligned} P^{\text{el}, M_L, \eta, \gamma} &= P_{n_1 n_2, n_1 n_2}^{M_L, \eta, \gamma} \\ P^{\text{in}, M_L, \eta, \gamma} &= \sum_{n'_1 n'_2 \neq n_1 n_2} P_{n'_1 n'_2, n_1 n_2}^{M_L, \eta, \gamma} \\ P^{\text{re}, M_L, \eta, \gamma} &= 1 - P^{\text{el}, M_L, \eta, \gamma} - P^{\text{in}, M_L, \eta, \gamma}. \end{aligned} \quad (27)$$

We mean by “inelastic”, processes that change the external confining states of the molecules. Finally, for an initial state $n_1 n_2$, the elastic, inelastic, and reactive cross sections are given by [34–36]

$$\begin{aligned} \sigma_{n_1 n_2}^{\text{el}} &= \frac{\hbar}{\sqrt{2\mu E_c}} \sum_{M_L, \eta, \gamma} |1 - S_{n_1 n_2, n_1 n_2}^{M_L, \eta, \gamma}|^2 \times \Delta \\ \sigma_{n_1 n_2}^{\text{in}} &= \frac{\hbar}{\sqrt{2\mu E_c}} \sum_{M_L, \eta, \gamma} P^{\text{in}, M_L, \eta, \gamma} \times \Delta \\ \sigma_{n_1 n_2}^{\text{re}} &= \frac{\hbar}{\sqrt{2\mu E_c}} \sum_{M_L, \eta, \gamma} P^{\text{re}, M_L, \eta, \gamma} \times \Delta. \end{aligned} \quad (28)$$

The inelastic state-to-state cross section is given by

$$\sigma_{n_1 n_2 \text{ to } n'_1 n'_2}^{\text{in}} = \frac{\hbar}{\sqrt{2\mu E_c}} \sum_{M_L, \eta, \gamma} P_{n'_1 n'_2, n_1 n_2}^{M_L, \eta, \gamma} \times \Delta. \quad (29)$$

The factor Δ represents symmetrization requirements for indistinguishable particles in a same internal and confining state [11, 37]. The cross sections are found by summing over all the contributions of different values of M_L, η, γ . For the ultralow energies involved in this study, only the first partial wave will be required for indistinguishable molecules (same internal states $\eta = +1$

and same confining state $\gamma = +1$): the $M_L = 0$ partial wave for indistinguishable bosons and the $M_L = \pm 1$ partial wave for indistinguishable fermions. The temperature dependence of the loss rates in the two dimensional plane is found by averaging the cross sections over a two-dimensional Maxwell-Boltzmann distribution of the relative velocity $v = \sqrt{2E_c/\mu}$ in the two-dimensional plane. This gives a two dimensional thermalized rate

$$\beta_{n_1 n_2}^{T, \text{el, in, re}} = \int_0^\infty \sigma_{n_1 n_2}^{\text{el, in, re}} v f(v) dv \quad (30)$$

with

$$f(v) = \frac{\mu}{k_B T} v e^{-\frac{\mu v^2}{2k_B T}} \quad (31)$$

where k_B is the Boltzmann constant. The rate in Eq. 30 corresponds to the rate per molecule, not the event or collision rate [11, 37].

Selection rules apply due to symmetrization of the wavefunction under permutation of identical molecules (Appendix C). The rules are

$$\eta \gamma (-1)^{M_L} = \eta (-1)^L = \eta (-1)^{M_L + n} = \epsilon_P. \quad (32)$$

This limits the summation over M_L, η, γ in Eq. (28) and (30) and the values of the quantum numbers j'' and n'' used in Eq. (11) and Eq. (17).

In the following, we will consider molecules of KRb as an illustrative example of experimental interest [1, 2, 5, 22]. For concreteness, we will take the isotope $^{39}\text{K}^{87}\text{Rb}$ for the bosonic molecules; the results for the bosonic isotope $^{41}\text{K}^{87}\text{Rb}$ [5] are nearly identical. We take the isotope $^{40}\text{K}^{87}\text{Rb}$ for the fermionic molecules [1, 2, 22]. Convergence of the results have been checked with the matching distance r_{max} and the number of adiabatic functions N_{adiab} included in the expansion of the wavefunction. Unless stated otherwise, we choose $r_{\text{min}} = 10 a_0$ and $r_{\text{max}} = 10000 a_0$ ($a_0 \simeq 0.529$ Angstroms is the Bohr radius), $N_s = 10000$ sectors, $0 < n_1, n_2 < n_{\text{osc}}^{\text{max}} = 3$, $N_{\text{adiab}} = 2 n_{\text{osc}}^{\text{max}} = 6$ and only the first partial waves $M_L = 0, 1$ depending on the species and the selection rules involved. We used $N_l = 80$ Legendre polynomials for $\nu < 100$ kHz and $N_l = 120$ for $\nu \geq 100$ kHz, to construct the adiabatic functions. This yields converged results of 10 % at most for the elastic rates (more especially at high confinement) and 1 % for the reactive and inelastic rates. For V_{abs} , we use $A = -10$ K and $r_c = 10 a_0$, which adequately reproduces experimental loss rates in three dimensional collisions [2].

III. SUPPRESSION OF CHEMICAL REACTIONS

We discuss in this section how chemical reactions proceed when the reactants are subject to different confinements and electric fields. We present in Fig. 2 the adiabatic energies $\epsilon_j(r_p)$ for the symmetry $\gamma(-1)^{M_L} = -1$

(upper panel) and the symmetry $\gamma(-1)^{M_L} = +1$ (lower panel), for a trap with $\nu = 20$ kHz and induced dipole moment $d = 0.1$ D. These energies converge at large r to the energies of the relative harmonic oscillator ϵ_n . To associate a specific confined collision with a symmetry $\gamma(-1)^{M_L}$, one has to use Eq. (32). If the molecules are identical fermions in the same internal state, $\eta = +1$ and $\epsilon_P = -1$, and then $\gamma(-1)^{M_L} = -1$, so the scattering problem only employs the black and red dashed curves of the upper panel in Fig. 2. In addition, if the identical fermionic molecules are in the same external state, then $\gamma = +1$, and the scattering problem only uses the black curves. If however the identical fermionic molecules are in different internal states, both values of η are relevant. Then, in the case of $\eta = -1$, now $\gamma(-1)^{M_L} = +1$, and the black and red dashed curves of the lower panel have to be employed as well. If the fermionic molecules are in different internal states, but in the same external state, then $\gamma = +1$, and one has to use only the black curves of both panels.

Using similar arguments, if molecules are identical bosons in the same internal state, one has to use the black and red dashed curves of the lower panel. If besides they are in the same external state, only the black curves have to be used. If they are in different internal states, all black and red dashed curves of both panels have to be used, while only the black curves of both panels are used if the identical bosons are in different internal states but in the same external state. The case of two different polar molecules corresponds to all curves of all symmetries employed. Also, note that because $\gamma(-1)^{M_L} = (-1)^L = (-1)^{M_L + n}$ in Eq. (32), the values of L and $M_L + n$ are odd for the upper panel and even for the lower panel, and the $\gamma = +1$ ($\gamma = -1$) curves corresponds to even (odd) relative quantum numbers n ($\gamma = (-1)^n$). Therefore, symmetry consideration are essential for the dynamics of ultracold molecules in confined geometry and electric field.

We now discuss the differences between the symmetries rather than a specific confined collisional case. We focus on the symmetry $\gamma(-1)^{M_L} = -1$ with $\gamma = +1$ (black curves of the upper panel in Fig. 2) and on the symmetry $\gamma(-1)^{M_L} = +1$ with $\gamma = +1$ (black curves of the lower panel in Fig. 2). The former case corresponds to the dynamics of identical indistinguishable fermions and the latter to the dynamics of identical indistinguishable bosons. By indistinguishable, we mean identical molecules in the same internal and external states. For the discussion, we focus only on the lowest black curve if we assume molecules in the ground state of the trapping potential. Two striking differences can be seen due to the statistics of the systems. First, the lowest curve connects at short distance to an adiabatic curve with a $L = 1$ adiabatic barrier V_b (depicted with a green arrow) for the $\gamma(-1)^{M_L} = -1$ symmetry (upper panel), while no barrier is present ($L = 0$) for the $\gamma(-1)^{M_L} = +1$ symmetry (lower panel). This

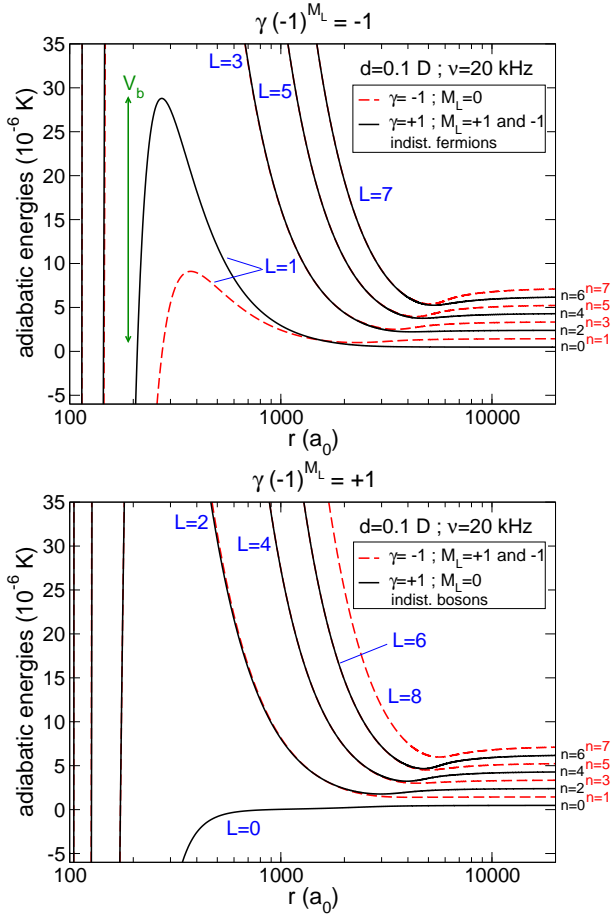


FIG. 2: (Color online) Adiabatic energies versus r for the $\gamma(-1)^{M_L} = -1$ symmetry (upper panel) and for the $\gamma(-1)^{M_L} = +1$ symmetry (lower panel), for $\nu = 20$ kHz and $d = 0.1$ D. The black (red dashed) curves correspond to $\gamma = +1$ ($\gamma = -1$) manifolds. We also show how values of L and n adiabatically connect. V_b is the height of the barrier for molecules in the lowest confining state ($n = 0$).

makes indistinguishable bosonic molecules likely to chemically react in confined geometry compared to fermionic molecules. Second, the lowest curve ($\gamma = +1$) corresponds to $M_L = \pm 1$ for the first symmetry while it corresponds to $M_L = 0$ for the second one. Under an electric field, the $M_L = 0$ component always corresponds to an attractive dipole-dipole interaction whereas the $M_L = 1$ component corresponds to a repulsive dipole-dipole interaction (which can eventually turn into an attractive one at higher dipoles [2, 11]). For this rather small confinement, it means that we can still, up to a certain dipole, use an electric field to increase the barrier V_b for indistinguishable fermions. This is not true for indistinguishable bosons. We will refer to this kind of suppression as “statistical suppression”, as it depends on the fermionic/bosonic character. To get suppression for indistinguishable bosons, we will have to increase the confinement and the electric field, which will be referred

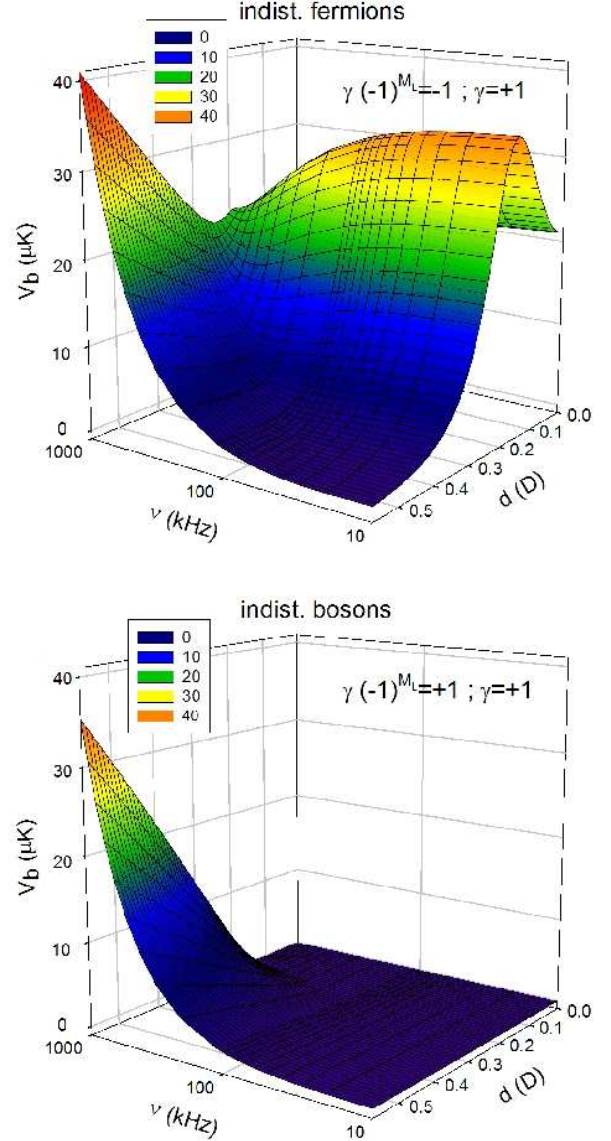


FIG. 3: (Color online) Height of the adiabatic barrier V_b versus d and ν for indistinguishable fermions (upper panel) and for indistinguishable bosons (lower panel) in the lowest confining state.

in the following to as “potential energy suppression”.

To understand these two types of suppression, it is useful to plot the height of the barrier V_b , which the molecules at ultralow temperature must tunnel through. We plot this barrier in Fig. 3 for the symmetry $\gamma(-1)^{M_L} = -1$ with $\gamma = +1$ (upper panel) and for the symmetry $\gamma(-1)^{M_L} = +1$ with $\gamma = +1$ (lower panel), as a function of the confinement ν and the dipole moment d induced by the electric field, for the lowest confining state. For the first symmetry (upper panel), there are two ways to get a high barrier. One way is for small

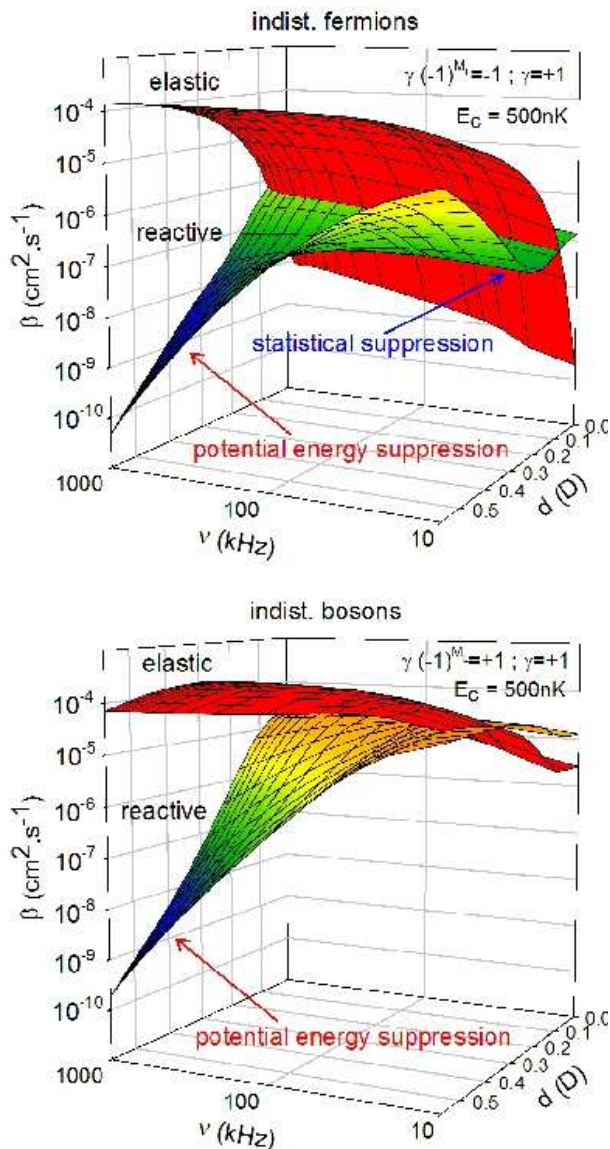


FIG. 4: (Color online) Elastic and reactive rate coefficient versus d and ν for indistinguishable fermions (upper panel) and for indistinguishable bosons (lower panel) at $E_c = 500$ nK. The elastic curve is plotted in red.

confinements and small d . The barrier increases to reach a maximum at $d \approx 0.15$ D. The fact that the barrier decreases for higher dipoles comes from contributions of higher values of $L = 3, 5, \dots$ [2, 11]. For $d \approx 0.15$ D, if we follow this maximum of the three-dimensional plot for increasing confinements, we see that V_b decreases again. When ν increases, the zero-point energies (the ones at large r in Fig. 2) increase while the barrier is not affected at short distance because the confinement is small. Then, the effective height of the barrier is decreased [15] as ν increases. The second way to achieve high barriers V_b is for high dipoles and high confinements. The barrier

increases monotonically, emphasizing the electric field suppression of confined chemical rates. When the molecules are highly confined in a two dimensional plane perpendicular to an applied electric field, they collide side-by-side. This repulsive electric interaction enhances the barrier and makes the molecules stable against collisions [12–17].

For the second symmetry (lower panel), there is only one way to increase the barrier. The striking difference is that for small confinement and/or small dipoles, there is no barrier at short range as already seen in Fig. 2. The only way to raise the barrier is for high confinements and high dipoles as for the first symmetry, where the electric dipole repulsion come into play. The rise of the barrier at high confinements and high dipoles is independent of the symmetrization of the molecules, as V_b converges to similar values for both cases.

The behavior of V_b has crucial consequences on the dynamics of the molecules. To get the rate coefficients of a specific confined collision, one has to add the rates obtained from a scattering calculation using the adiabatic curves of the individual symmetries $\gamma(-1)^{M_L}$ involved in the specific problem. The rates for the symmetry $\gamma(-1)^{M_L} = -1$ with $\gamma = +1$ is presented in the upper panel and for the symmetry $\gamma(-1)^{M_L} = +1$ with $\gamma = +1$ in the lower panel of Fig. 4, as a function of ν and d for a collision energy $E_c = 500$ nK. Qualitatively, the behavior of the reactive rates is opposite to the height of the corresponding barriers, while the elastic rates increase only in a monotonic way with d and ν . For small confinements and dipoles (say $\nu = 20$ kHz, $d = 0.15$ D), the reactive rates are suppressed for the first symmetry (upper panel) representing approximately 10^{-2} of the elastic rates. No such suppression is seen for the second symmetry (lower panel). This shows that this statistical suppression is only due to symmetrization requirements, but has the advantage to work at rather realistic experimental confinements and dipoles. For high confinements and dipoles, the reactive rates of fermions and bosons can be suppressed by three to four orders of magnitude compared to the ones at small confinements. This is made possible by the anisotropy of the dipolar interaction of polar molecules in confined geometries as explained in Refs. [12–17].

The elastic rates increase as d^4 or d , depending on the collision energy and magnitude of the dipole [39], and increase with ν [15, 16]. Therefore, this potential energy suppression of the reactive rates and enhancement of the elastic processes will help evaporative cooling of fermionic and bosonic molecules, and will make amenable the creation of degenerate Fermi gases or Bose–Einstein condensates of polar molecules. This suppression is not due to symmetrization requirements but to the fact that the molecules possess a permanent electric dipole moment. Therefore, this suppression will also be effective for molecules in distinguishable states or even for non-identical polar molecules.

It is worth noting that the fermionic statistical sup-

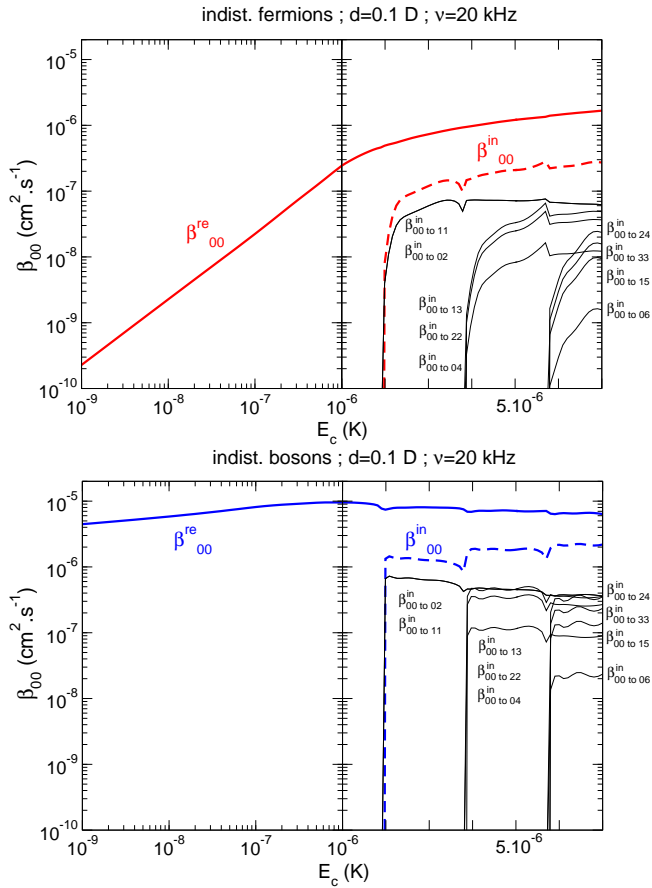


FIG. 5: (Color online) Rate coefficient $\beta_{00}^{\text{in, re}}$ versus collision energy E_c for $d = 0.1$ D and $\nu = 20$ kHz, for indistinguishable fermions (upper panel) and indistinguishable bosons (lower panel), initially in the ground state of the confining trap $n_1 = n_2 = 0$. The thick solid (dashed) curve corresponds to reactive (inelastic) scattering. The thin solid black lines represent the confining state-to-state rate coefficients.

pression is still effective if the fermions are in different external states ($\gamma = \pm 1$), since both black and red dashed curves of the upper panel in Fig. 2 have to be used. The red curves corresponds to a $M_L = 0$ component, whose barrier height V_b decreases for increasing electric field. There is no statistical suppression at all if the molecules are in different internal states ($\eta = \pm 1$), because the curves from the lower panel in Fig. 2 have to be used including the barrierless curve $L = 0$. This has been confirmed experimentally [22].

Finally, no statistical suppression can occur in the case of different polar molecules, for which all curves of all symmetries in Fig. 2 should be employed. Only the potential energy suppression can apply in that case.

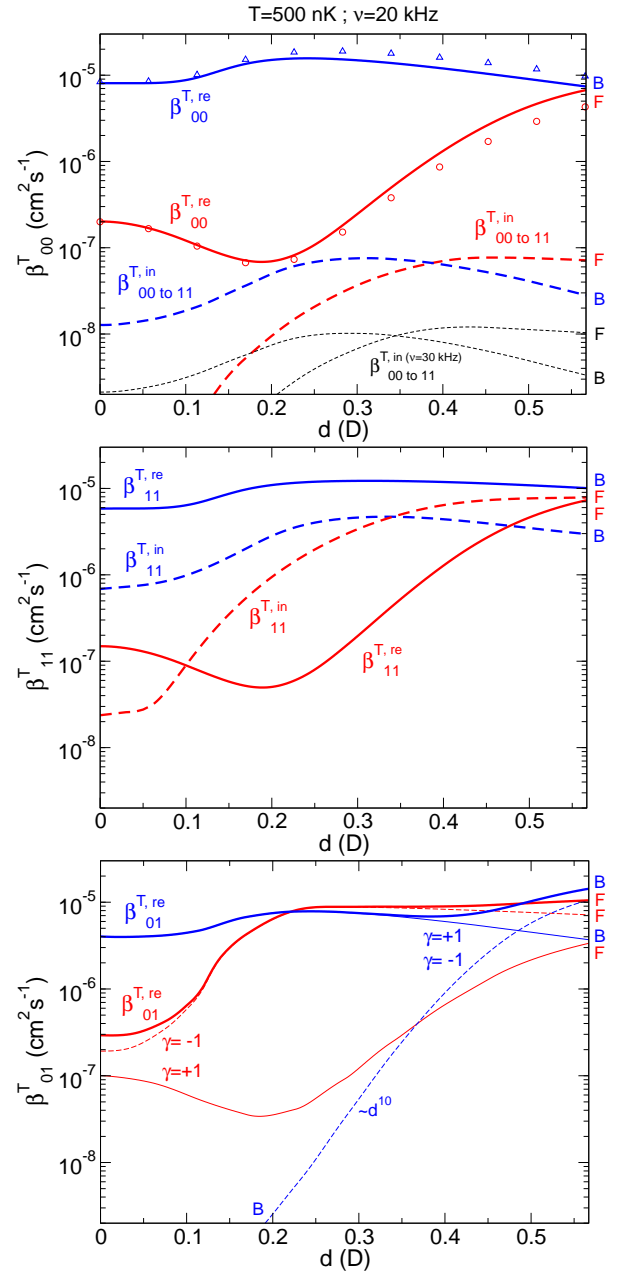


FIG. 6: (Color online) Thermalized rate coefficient versus d for $T = 500$ nK and $\nu = 20$ kHz. The solid (dashed) curves correspond to reactive (inelastic) processes. The red (blue) curves correspond to fermions (bosons) in same internal states, but not necessarily in same external states. The molecules are considered initially in $n_1 = 0, n_2 = 0$ (upper panel), in $n_1 = 1, n_2 = 1$ (middle panel), and in $n_1 = 0, n_2 = 1$ (lower panel).

IV. INELASTIC COLLISIONS BETWEEN CONFINING STATES

We saw that chemical suppression of indistinguishable fermions and bosons can always be obtained if suffi-

ciently high confinements and electric fields are applied. However, the magnitude of these high confinements is still beyond of those that can be currently achieved experimentally. For a realistic experimental frequency of $\nu \simeq 20$ kHz, loss of indistinguishable fermions can be suppressed taking advantage of the alternative statistical suppression whereas loss of indistinguishable bosons cannot realistically be suppressed. Moreover, for small confinements, it is possible that higher trap confining states can be populated. The reason is that the energy spacing between two allowed confining states $\Delta\varepsilon = 0.96 \mu\text{K}$ for $\nu \simeq 20$ kHz can be of the order of the temperature $T \simeq 500$ nK of the gas. Then, the changing-state dynamics of molecules in small confining optical lattices must be understood as well. We consider in the following fermions and bosons in same internal states but not necessarily in the same external confining states, for a realistic confinement of $\nu = 20$ kHz.

We present in Fig. 5 the non-thermalized rate coefficients $\beta_{00}^{\text{in, re}} = \sigma_{00}^{\text{in, re}} v$ as a function of the collision energy for the inelastic and reactive processes, for indistinguishable fermionic molecules (upper panel) and indistinguishable bosonic molecules (lower panel) in same internal and external states. The molecules start in $n_1 = 0$ and $n_2 = 0$ and $\nu = 20$ kHz, $d = 0.1$ D. States between $0 < n_1, n_2 < n_{\text{osc}}^{\text{max}} = 7$ have been used for collision energy $E_c > 1 \mu\text{K}$ to converge these results. At ultralow energy, the fermionic reactive rate scales as E_c , and as $\ln^{-2}(\sqrt{2\mu E_c})$ for the bosons, in agreement with the threshold laws [40, 41]. When the collision energy is sufficiently high, excited confining states become energetically open. Overall, bosons react at higher rate than fermions, as expected, since there is no barrier for bosons, whereas there is a barrier for fermions. Moreover, molecules that start in the ground confining state are much more likely to react chemically than to go to higher confining state. The inelastic rate for the fermionic molecules is an order of magnitude smaller than its reactive rate. It is a factor of 3 – 8 smaller than the reactive rate for the bosonic molecules.

A. Gas in thermal equilibrium

We now consider a thermal equilibrium at a temperature of $T = 500$ nK. The population p of the molecules in n_τ is given by a Maxwell-Boltzmann distribution

$$p(n_\tau) = \frac{e^{-\frac{\varepsilon_{n_\tau}}{k_B T}}}{\sum_{n_\tau} e^{-\frac{\varepsilon_{n_\tau}}{k_B T}}}. \quad (33)$$

At $T = 500$ nK in a trap with $\nu = 20$ kHz, $p(n_\tau = 0) \simeq 0.852$, $p(n_\tau = 1) \simeq 0.126$ and $p(n_\tau = 2) \simeq 0.019$. In the following we will neglect contribution of molecules in $n_\tau = 2$, and consider only molecules in $n_\tau = 0, 1$ for simplification. The coefficients $p(n_\tau)$ will play a role in the rate equations

below.

We present in Fig. 6 the thermalized rates $\beta_{00}^{T, \text{re}}$ and $\beta_{00}^{T, \text{in}}$ (upper panel), $\beta_{11}^{T, \text{re}}$ and $\beta_{11}^{T, \text{in}}$ (middle panel), and $\beta_{01}^{T, \text{re}}$ (lower panel), as a function of d for $\nu = 20$ kHz at $T = 500$ nK. The reactive and inelastic rates are plotted as a thick and dashed solid line. The fermionic and bosonic case are plotted in red and blue respectively.

We discuss first the case of molecules in the ground states $n_1 = 0, n_2 = 0$ (upper panel). For bosons, the reactive rate is high and the inelastic collision is insignificant. For fermions however, the inelastic rate can reach 20 % of the amount of the reactive rate at $d = 0.23$ D. The magnitude of the thermalized inelastic rates is proportional to the amount of molecules allowed by the Maxwell-Boltzmann distribution at $T = 500$ nK to have kinetic energy greater than the first excited inelastic thresholds $n_1 = 1, n_2 = 1$ and $n_1 = 0, n_2 = 2$ at $1.92 \mu\text{K}$. We also plot in circles (fermions) and triangles (bosons) the non-thermalized reactive rate $\beta_{00}^{\text{re}} = \sigma_{00}^{\text{re}} v$. We see that $\beta_{00}^{T, \text{re}} = \beta_{00}^{\text{re}}$ is a reasonable approximation at small dipole moments. β_{00}^{re} differs by 35 % from $\beta_{00}^{T, \text{re}}$ at the highest dipole, however. This comes from the fact that at these dipoles, the molecules do not collide in the Wigner regime anymore and the height of the barrier for fermions (or characteristic energy for bosons) is comparable to the temperature. Note that if the confinement is increased to $\nu = 30$ kHz, the inelastic rate (represented as thin dashed black lines) decreases by about an order of magnitude, because for a same temperature, it is harder to excite molecules in higher confining states as the energy thresholds increases with the confinement. Then the inelastic collisions for ground state molecules become less important as the confinement increases.

If the molecules are now in the first excited states $n_1 = 1, n_2 = 1$ (middle panel), reactive collisions, for both bosons and fermions, are about 30 % smaller than the ones for molecules in $n_1 = 0, n_2 = 0$. A qualitative explanation is that $n_1 = 1, n_2 = 1$ (which has a $\gamma = +1$ symmetry) projects onto an $n = 0, N = 2$ state and a $n = 2, N = 0$ state (see Appendix B). When we look at the corresponding adiabatic energies in Fig. 2 for the fermions, the $n = 2$ curve connects to the $L = 3$ adiabatic barrier which is much higher than the $L = 1$ barrier, suppressing more strongly the reactive collisions and increasing inelastic collisions. For bosons, the reactive rates are still high compared to fermions, because the $n = 0$ curve connects to a $L = 0$ curve. However, the reactive rates are smaller than for the $n_1 = 0, n_2 = 0$ case, because there is now the $n = 2$ curve that connects to a $L = 2$ curve, suppressing chemical reactivity. The inelastic processes are much important in the present case because the Maxwell-Boltzmann distribution allows all molecules to have sufficient kinetic energy to contribute to the inelastic process, while in the precedent case, only a part of the molecules were allowed to contribute to the inelastic process. For bosons, the inelastic magnitude is

about half the reactive rate (at most, at $d = 0.3$ D), but for fermions, it can even exceed the reactive rate for $d > 0.1$ D.

Finally, we discuss the case of molecules in different states $n_1 = 0, n_2 = 1$ (lower panel). This channel cannot decay to the energetically allowed $n_1 = 0, n_2 = 0$ channel, because the two channels correspond to different values of N . However, the molecules are in different confining states now so that two contributions $\gamma = \pm 1$ are involved in the calculation, and both black and red dashed curves of Fig. 2 have to be used. This is shown in the lower panel of Fig. 6 as thin solid line for $\gamma = +1$ and thin dashed line for $\gamma = -1$. Compared to fermionic molecules in the same confining states, the reactive rates are bigger. This comes mainly from the $\gamma = -1$ contribution, which corresponds to $M_L = 0$ head-to-tail attractive dipolar interactions (see Tab. I). For bosonic molecules in different confining states, the reactive rates are similar to those for molecules in same confining states, except that the $\gamma = -1$ contribution gives an enhancement at high dipoles due to the $M_L = 1$ component of the $L = 2$ adiabatic curve (see Tab. I). This component corresponds to an attractive dipolar interaction (see Eq. 8 and Eq. 9 of Ref. [11]) and can enhance the reactive rate at high dipoles. The $L = 2$ barrier is high at small dipoles (see Fig. 2) and suppresses the reactive rates. However, the strong dependence of $d^{4(L+1/2)}$ of the rates [11] leads to a d^{10} dependence, as shown in the figure, and eventually makes a significant contribution at high dipoles.

We saw on one hand that inelastic processes can be important for molecules initially in excited confining states, especially for fermions, and that on the other hand molecules can chemically react at high rates for molecules initially in different confining states, even for fermions because they are not indistinguishable anymore. What are the consequences of this for the dynamics of a molecular gas? This is what we answer in the next subsection.

B. Rate equations

The rate equations for the density of molecules $n_{n_\tau}(t)$ in state n_τ as a function of time are given by

$$\begin{aligned} \dot{n}_0(t) &= -\beta_{00}^{T,\text{re}} n_0^2(t) - \beta_{01}^{T,\text{re}} n_0(t) n_1(t) \\ &\quad - \beta_{00\text{to}11}^T n_0^2(t) + \beta_{11\text{to}00}^T n_1^2(t) \\ \dot{n}_1(t) &= -\beta_{11}^{T,\text{re}} n_1^2(t) - \beta_{01}^{T,\text{re}} n_0(t) n_1(t) \\ &\quad - \beta_{11\text{to}00}^T n_1^2(t) + \beta_{00\text{to}11}^T n_0^2(t) \end{aligned} \quad (34)$$

where $n_0(t)$ ($n_1(t)$) are the individual densities of molecules in state $n_\tau = 0$ ($n_\tau = 1$). Similar equations hold for $n_\tau \geq 2$, but for simplicity, to avoid additional inelastic terms in the equations, we assumed $p_{n_\tau \geq 2} \ll p_{n_\tau=0,1}$.

If we assume a gas in thermal equilibrium for each time t , the Maxwell-Boltzmann distribution implies that $n_0(t) = p(0) n_{\text{tot}}(t)$ and $n_1(t) = p(1) n_{\text{tot}}(t)$ (we assume

$p(0) + p(1) \simeq 1$ in our example), where $n_{\text{tot}}(t)$ is the density of the total molecules. Then by summing the equations above, we obtain the rate equation for $n_{\text{tot}}(t)$

$$\begin{aligned} \dot{n}_{\text{tot}}(t) &= -\left\{ p^2(0) \beta_{00}^{T,\text{re}} + p^2(1) \beta_{11}^{T,\text{re}} \right. \\ &\quad \left. + 2p(0)p(1) \beta_{01}^{T,\text{re}} \right\} n_{\text{tot}}^2(t). \end{aligned} \quad (35)$$

Inelastic rates cancel each other in the full equation, because two molecules go back and forth in $n_1 = 0, n_2 = 0$ and $n_1 = 1, n_2 = 1$, without participating in the loss process. Although inelastic collisions are responsible for the evolution of the individual density of molecules $n_0(t)$ and $n_1(t)$, they are not responsible for the evolution of the total density of molecules in the thermal gas.

At $T = 500$ nK, $\beta_{11}^{T,\text{re}} \simeq \beta_{00}^{T,\text{re}}$ but $p^2(1) \ll p^2(0)$ so that the second term on the right hand side of the equation above can be neglected. As a result the density of the total molecules will show a faster decay due to a fast rate $2p(0)p(1)\beta_{01}^{T,\text{re}}$ and a slow decay due to a slow rate $p^2(0)\beta_{00}^{T,\text{re}}$. For example for fermionic KRb at $d = 0.2$ D, $2p(0)p(1)\beta_{01}^{T,\text{re}} \simeq 1.4 \cdot 10^{-6} \text{ cm}^2 \text{ s}^{-1}$ and $p^2(0)\beta_{00}^{T,\text{re}} \simeq 5 \cdot 10^{-8} \text{ cm}^2 \text{ s}^{-1}$. The fast and slow decays are due to high inter-states reactive rates (collisions between different confining states) and low intra-states reactive rates (collisions between same confining states). The two types of decay can be tuned by changing the relative populations $p(0)$ and $p(1)$, by changing the temperature T and/or the confinement ν . Note that even if the population of the molecules in different confining states are not given by a Maxwell-Boltzmann distribution, say for example $p(0) = 0.5$ and $p(1) = 0.5$, and is independent of time, inelastic rates still cancel each other in the equation for the total density of molecules. Again, inelastic collisions play a role in the loss of molecules from individual trap levels, but do not for the loss of the total molecules. These theoretical findings well support recent experimental data of confined fermionic KRb molecules in electric fields [22].

V. CONCLUSION

We have developed in detail a rigorous time-independent quantum formalism to describe the dynamics of particles with permanent electric dipole moments in a confined geometry, by treating the reactive chemistry using an absorbing potential. Elastic, reactive and inelastic rate coefficients can be computed for a given collision energy, temperature, confinement and dipole moment (or electric field), for a system of fermionic or bosonic molecules. The selection rules play an important role for the dynamics of confined molecules and have dramatic effects on the collisional properties. Different rates are obtained for fermionic/bosonic molecules in same/different confining states. Two kinds of suppression can occur for chemical reactions: a statistical suppression applies only

for fermions at rather small induced dipoles and confinements realistically accessible in an experiment, and a potential energy suppression applies for both fermions and bosons at rather high induced dipoles and confinements. Inelastic rates can be important, even as high as reactive rates for molecules initially in excited states. However, the inelastic rates do not play a role in the loss process of the total number of molecules in a gas, since molecules are inelastically excited and relaxed, back and forth. Only reactive rates are responsible for the evolution of the loss of the total molecules. Fast and slow decays of the molecules can be seen due to inter-state and intra-state confined collisions. This work has been highly motivated by recent experiments of KRb molecules in confined geometry and electric field, and has proved very good theoretical support for the experimental observations [22].

Acknowledgments

This material is based upon work supported by the Air Force Office of Scientific Research under the Multidisciplinary University Research Initiative Grant No. FA9550-09-1-0588. We also acknowledge the financial support of the National Institute of Standards and Technology and the National Science Foundation. We thank M. H. G. de Miranda, A. Chotia, B. Neyenhuis, D. Wang, S. Ospelkaus, S. Moses, D. S. Jin and J. Ye for stimulating discussions about the KRb experiment.

Appendix A: Relation between $|n_1 n_2\rangle$ and $|n, N\rangle$

In Eq. (7), we use the following characteristics [42]

$$g_{n_\tau}(x) = \sqrt{\frac{1}{2^{n_\tau} n_\tau!}} \left(\frac{m_\tau \omega}{\pi \hbar}\right)^{1/4} e^{-\frac{m_\tau \omega x^2}{2\hbar}} H_{n_\tau}(\sqrt{m_\tau \omega/\hbar} x) \quad (36)$$

$$H_{n_\tau}(x+y) = 2^{-n_\tau/2} \sum_{k=0}^n \frac{n_\tau!}{k!(n_\tau-k)!} H_k(x\sqrt{2}) H_{n_\tau-k}(y\sqrt{2}) \quad (37)$$

$$H_{n_\tau}(x) H_{m_\tau}(x) = \sum_{k=0}^{\min(n_\tau, m_\tau)} \frac{m_\tau!}{k!(m_\tau-k)!} \frac{n_\tau!}{k!(n_\tau-k)!} H_{-2k+m_\tau+n_\tau}(x) 2^k k!. \quad (38)$$

The individual $|n_1 n_2\rangle$ states are written in terms of

the relative/CM $|n, N\rangle$ states by

$$\begin{aligned} |00\rangle &= |0, 0\rangle \\ |01\rangle &= \frac{1}{\sqrt{2}}|0, 1\rangle + \frac{1}{\sqrt{2}}|1, 0\rangle \\ |10\rangle &= \frac{1}{\sqrt{2}}|0, 1\rangle - \frac{1}{\sqrt{2}}|1, 0\rangle \\ |02\rangle &= \frac{1}{2}|0, 2\rangle + \frac{1}{\sqrt{2}}|1, 1\rangle + \frac{1}{2}|2, 0\rangle \\ |20\rangle &= \frac{1}{2}|0, 2\rangle - \frac{1}{\sqrt{2}}|1, 1\rangle + \frac{1}{2}|2, 0\rangle \\ |11\rangle &= \frac{1}{\sqrt{2}}|0, 2\rangle - \frac{1}{\sqrt{2}}|2, 0\rangle. \end{aligned} \quad (39)$$

Appendix B: Relation between $|n_1 n_2, \gamma\rangle$ and $|n, N\rangle$

Using Eq. (5) and Appendix A, the symmetrized individual $|n_1 n_2, \gamma\rangle$ states are written in terms of the relative/CM $|n, N\rangle$ states by

$$\begin{aligned} |00, \gamma = +1\rangle &= |0, 0\rangle \\ |01, \gamma = +1\rangle &= |0, 1\rangle \\ |02, \gamma = +1\rangle &= \frac{1}{\sqrt{2}}|0, 2\rangle + \frac{1}{\sqrt{2}}|2, 0\rangle \\ |11, \gamma = +1\rangle &= \frac{1}{\sqrt{2}}|0, 2\rangle - \frac{1}{\sqrt{2}}|2, 0\rangle \\ |12, \gamma = +1\rangle &= \sqrt{\frac{12}{16}}|0, 3\rangle - \frac{1}{2}|2, 1\rangle \\ |22, \gamma = +1\rangle &= \sqrt{\frac{3}{8}}|0, 4\rangle - \frac{1}{2}|2, 2\rangle + \sqrt{\frac{3}{8}}|4, 0\rangle \\ |01, \gamma = -1\rangle &= |1, 0\rangle \\ |02, \gamma = -1\rangle &= |1, 1\rangle \\ |12, \gamma = -1\rangle &= \frac{1}{2}|1, 2\rangle - \sqrt{\frac{12}{16}}|3, 0\rangle. \end{aligned} \quad (40)$$

Note that $(-1)^{n_1+n_2} = (-1)^{n+N}$.

fermions	η	L	γ	M_L	n
	+1	1,3,5 ...	+1	1,3,5 ...	0,2,4 ...
		1,3,5 ...	-1	0,2,4 ...	1,3,5 ...
	-1	0,2,4 ...	+1	0,2,4 ...	0,2,4 ...
		2,4,6 ...	-1	1,3,5 ...	1,3,5 ...
bosons	η	L	γ	M_L	n
	+1	0,2,4 ...	+1	0,2,4 ...	0,2,4 ...
		2,4,6 ...	-1	1,3,5 ...	1,3,5 ...
	-1	1,3,5 ...	+1	1,3,5 ...	0,2,4 ...
		1,3,5 ...	-1	0,2,4 ...	1,3,5 ...

TABLE I: Selection rules for the dynamics of identical bosons and fermions in confined two dimensional geometry.

Appendix C: Selection rules

For initial states n_1, n_2 and final states n'_1, n'_2 , since components of different N do not mix together in the collision process, we have

$$(-1)^{n_1+n_2} = (-1)^{n'_1+n'_2} \quad (41)$$

after a collision.

At long range, in cylindrical coordinates, if we use the symmetrized individual representation $|n_1 n_2, \gamma\rangle$, the permutation P requires the substitutions $z_1 \rightarrow z_2, z_2 \rightarrow z_1, \varphi \rightarrow \varphi + \pi$ which leads to the selection rule

$$\eta \gamma (-1)^{M_L} = \epsilon_P. \quad (42)$$

If we use the relative representation $|n, N\rangle$ states, then the permutation P requires the substitutions $z \rightarrow -z, \varphi \rightarrow \varphi + \pi$ which leads to

$$\eta (-1)^{M_L+n} = \epsilon_P, \quad (43)$$

from the properties of the $g_n(z)$ functions. At short range, in spherical coordinates, using the Legendre polynomials, the permutation P requires the substitutions $\theta \rightarrow \pi - \theta, \varphi \rightarrow \varphi + \pi$ which leads to

$$\eta (-1)^L = \epsilon_P. \quad (44)$$

We summarize in Tab. I the different selection rules for identical bosons and fermions.

-
- [1] S. Ospelkaus, K.-K. Ni, D. Wang, M. H. G. de Miranda, B. Neyenhuis, G. Quémener, P. S. Julienne, J. L. Bohn, D. S. Jin, and J. Ye, *Science* **327**, 853 (2010).
- [2] K.-K. Ni, S. Ospelkaus, D. Wang, G. Quémener, B. Neyenhuis, M. H. G. de Miranda, J. L. Bohn, J. Ye, and D. S. Jin, *Nature*, **464** 1324 (2010).
- [3] K.-K. Ni, S. Ospelkaus, M. H. G. de Miranda, A. Pe'er, B. Neyenhuis, J. J. Zirbel, S. Kotochigova, P. S. Julienne, D. S. Jin, and J. Ye, *Science* **322**, 231 (2008).
- [4] S. Ospelkaus, K.-K. Ni, G. Quémener, B. Neyenhuis, D. Wang, M. H. G. de Miranda, J. L. Bohn, J. Ye, and D. S. Jin, *Phys. Rev. Lett.* **104**, 030402 (2010).
- [5] K. Aikawa, D. Akamatsu, M. Hayashi, K. Oasa, J. Kobayashi, P. Naidon, T. Kishimoto, M. Ueda, and S. Inouye, accepted to *Phys. Rev. Lett.*, arXiv:1008.5034.
- [6] J. M. Sage, S. Sainis, T. Bergeman, and D. DeMille, *Phys. Rev. Lett.* **94**, 203001 (2005).
- [7] J. Deiglmayr, A. Grochola, M. Repp, K. Mörtlbauer, C. Glück, J. Lange, O. Dulieu, R. Wester, and M. Weidemüller, *Phys. Rev. Lett.* **101**, 133004 (2008).
- [8] P. S. Żuchowski and J. M. Hutson, *Phys. Rev. A* **81**, 060703(R) (2010).
- [9] J. N. Byrd, J. A. Montgomery Jr., and R. Côté, *Phys. Rev. A* **82**, 010502(R) (2010).
- [10] E. R. Meyer and J. L. Bohn, accepted to *Phys. Rev. A*, arXiv:1004.3317.
- [11] G. Quémener and J. L. Bohn, *Phys. Rev. A* **81**, 022702 (2010).
- [12] H. P. Büchler, E. Demler, M. Lukin, A. Micheli, N. Prokofiev, G. Pupillo, and P. Zoller, *Phys. Rev. Lett.* **98**, 060404 (2007).
- [13] A. Micheli, G. Pupillo, H. P. Büchler, and P. Zoller, *Phys. Rev. A* **76**, 043604 (2007).
- [14] C. Ticknor, *Phys. Rev. A* **81**, 042708 (2010).
- [15] G. Quémener and J. L. Bohn, *Phys. Rev. A* **81**, 060701(R) (2010).
- [16] A. Micheli, Z. Idziaszek, G. Pupillo, M. A. Baranov, P. Zoller, and P. S. Julienne *Phys. Rev. Lett.* **105**, 073202 (2010).
- [17] J. P. D'Incao and C. H. Greene, in preparation.
- [18] L. D. Carr, D. DeMille, R. V. Krems, and J. Ye, *New J. Phys.* **11**, 055049 (2009).
- [19] A. Micheli, G. K. Brennen and P. Zoller, *Nat. Phys.* **2**, 341 (2006).
- [20] D. DeMille, *Phys. Rev. Lett.* **88**, 067901 (2002).
- [21] S. F. Yelin, K. Kirby, and R. Côté, *Phys. Rev. A* **74**, 050301(R) (2006).
- [22] M. H. G. de Miranda, A. Chotia, B. Neyenhuis, D. Wang, G. Quémener, S. Ospelkaus, J. L. Bohn, J. Ye, and D. S. Jin, submitted.
- [23] D. S. Petrov and G. V. Shlyapnikov, *Phys. Rev. A* **64**, 012706 (2001).
- [24] Z. Li and R. V. Krems, *Phys. Rev. A* **79**, 050701(R) (2009).
- [25] B. E. Granger and D. Blume, *Phys. Rev. Lett.* **92**, 133202 (2004).
- [26] P. F. O'Mahony and F. Mota-Furtado, *Phys. Rev. Lett.* **67**, 2283 (1991).
- [27] P. Soldán, *Phys. Rev. A* **82**, 034701 (2010).
- [28] R. T Pack and G. A. Parker, *J. Chem. Phys.* **87**, 3888 (1987).
- [29] J.-M. Launay and M. Le Dourneuf, *Chem. Phys. Lett.* **163**, 178 (1989).
- [30] G. Quémener, PhD Thesis, University of Rennes, France (2006), <http://tel.archives-ouvertes.fr/tel-00204105>.
- [31] Z. Idziaszek and P. S. Julienne *Phys. Rev. Lett.* **104**, 113202 (2010).
- [32] Z. Idziaszek, G. Quémener, J. L. Bohn and P. S. Julienne, *Phys. Rev. A* **82**, 020703(R) (2010).
- [33] B. R. Johnson, *J. Comp. Phys.* **13**, 445 (1973).
- [34] I. Richard Lapidus, *Am. J. Phys.* **50**, 45 (1982).
- [35] S. K. Adhikari, *Am. J. Phys.* **54**, 362 (1986).
- [36] P. Naidon and P. S. Julienne, *Phys. Rev. A* **74**, 062713 (2006).
- [37] J. P. Burke, Jr., PhD Thesis, University of Colorado (1999), <http://jilawww.colorado.edu/pubs/thesis/burke>.
- [38] M. Abramowitz and I. A. Stegun, *Handbook of mathematical functions*, Dover editions.
- [39] C. Ticknor, *Phys. Rev. A* **80**, 052702 (2009).
- [40] H. R. Sadeghpour, J. L. Bohn, M. J. Cavagnero, B. D. Esry, I. I. Fabrikant, J. H. Macek, and A. R. P. Rau, *J. Phys. B: At. Mol. Opt. Phys.* **33**, R93 (2000).
- [41] Z. Li, S. V. Alyabyshev, and R. V. Krems, *Phys. Rev. Lett.* **100**, 073202 (2008).
- [42] <http://functions.wolfram.com>